



Green, K., Krauskopf, B., & Engelborghs, K. (2004). One-dimensional unstable eigenfunction and manifold computations in delay differential equations. DOI: 10.1016/j.jcp.2003.11.018

Early version, also known as pre-print

Link to published version (if available):
[10.1016/j.jcp.2003.11.018](https://doi.org/10.1016/j.jcp.2003.11.018)

[Link to publication record in Explore Bristol Research](#)
PDF-document

University of Bristol - Explore Bristol Research

General rights

This document is made available in accordance with publisher policies. Please cite only the published version using the reference above. Full terms of use are available:
<http://www.bristol.ac.uk/pure/about/ebr-terms.html>

One-dimensional unstable eigenfunction and manifold computations in delay differential equations

Kirk Green

*Department of Computer Science, K. U. Leuven, Celestijnenlaan 200A,
3001 Heverlee, Belgium*

Bernd Krauskopf

*Department of Engineering Mathematics, University of Bristol,
Bristol BS8 1TR, UK*

Koen Engelborghs

*Department of Computer Science, K. U. Leuven, Celestijnenlaan 200A,
3001 Heverlee, Belgium*

Abstract

In this paper we present a new numerical technique for computing the unstable eigenfunctions of a saddle periodic orbit in a delay differential equation. This is used to obtain the necessary starting data for the computation of one-dimensional unstable manifolds of an associated saddle fixed point of a suitable Poincaré map. To illustrate our method, we investigate an intermittent transition to chaos in a delay system describing a semiconductor laser subject to phase-conjugate feedback.

Key words: Numerical tools for DDEs, PCF laser, Intermittent transition
PACS: 02.30.Ks, 02.30.Oz, 02.70.-c, 42.65.Sf

Email addresses: `kirk.green@cs.kuleuven.ac.be` (Kirk Green),
`b.krauskopf@bristol.ac.uk` (Bernd Krauskopf),
`koen.engelborghs@cs.kuleuven.ac.be` (Koen Engelborghs).

1 Introduction

Numerical tools for the study of delay differential equations (DDEs) are of much interest to applied fields because models featuring a delay term appear in applications ranging from chemistry [9] and biology [2,26] to laser physics [21,29]. Until quite recently, the only techniques available to study DDEs were simulation by direct numerical integration of the DDE, or a linear stability analysis of steady states. This is now changing with the introduction of new tools for the numerical bifurcation analysis DDEs. At the fore of this new software is the continuation package DDE-BIFTOOL [8] allowing the user to find and follow steady states and periodic solutions in systems of DDEs irrespective of their stability; first examples of continuation studies with DDE-BIFTOOL can be found in Refs. [6,13–17,28].

In Ref. [20] we introduced the first method for computing one-dimensional (1D) unstable manifold of a saddle periodic orbit of a DDE with one unstable Floquet multiplier. Specifically, we compute (each branch) of the unstable manifold $W^u(q)$ of a saddle fixed point q of a suitable Poincaré map. For the computation of the two branches of $W^u(q)$, this method requires as starting data the saddle point q and two first points q_δ^\pm (one on each branch) approximately on $W^u(q)$ close to q . Using linear approximation near q , the points q_δ^\pm can be chosen some distance δ away from q along the unstable eigenspace $E^u(q)$. The saddle periodic orbit q can readily be found with DDE-BIFTOOL. For a DDE finding a good approximation of the first points q_δ^\pm is more difficult, and is the subject of this paper.

In Ref. [20] and the detailed study in Ref. [15] of the dynamics of a DDE describing a semiconductor laser subject to phase-conjugate feedback (PCF), also used here as an example and introduced in Section 4, we used an iterative power method to find a vector v approximately spanning the linear unstable eigenspace $E^u(q)$. This worked quite well and, by computing the invariant torus on which the dynamics of the PCF laser were locked, we were able to show that there is a transition to chaos culminated in a crisis bifurcation [15]. However, this iterative power method has its shortcomings; see Section 3 for details. In particular, we found that there are problems near bifurcations of the saddle periodic orbit, and in particular, close to regions of chaotic dynamics.

This realization motivated the present paper. We present here a method for obtaining the entire starting data for a manifold computation directly from a DDE-BIFTOOL computation. Specifically, we modified DDE-BIFTOOL to produce the unstable eigenfunction associated with the single unstable Floquet multiplier, this data is then used to find the points q_δ^\pm . This is less straightforward than it sounds owing to the infinite phase space of the DDE, and it requires several steps to get from the ‘raw data’ of DDE-BIFTOOL to a

suitable representation of q_δ^\pm .

To illustrate our technique we consider a sudden transition to chaos in the PCF laser caused by a saddle-node bifurcation of periodic orbits. In Ref. [19] this transition was found and identified by simulation and in Ref. [15] continuation techniques were used to follow periodic orbits to the saddle-node bifurcation. It appeared that the sudden transition to chaos is an *intermittent transition* [12,25], characterized by the saddle-node bifurcation taking place ‘on a chaotic attractor’. By this we mean, that one branch of the 1D unstable manifold of the saddle resembles the chaotic attractor that existed before the saddle-node bifurcation. Here we confirm the presence of an intermittent transition in a DDE for the first time by computing the unstable manifold of the saddle periodic orbit when this bifurcation is approached. This is only possible because we can now find much better starting data for the 1D manifold algorithm.

The paper is organized as follows. In Section 2 we introduce some background on the theory of DDEs. In Section 3 we explain how we find the starting data. Specifically, in Section 3.1 we detail how DDE-BIFTOOL is used to compute unstable eigenfunctions and in Section 3.2 we show how this eigenfunction data is manipulated to obtain the starting data for a manifold computation. As an illustration we show in Section 4 an intermittent transition to chaos in the PCF laser. Finally, we draw conclusions and discuss future work in Section 5.

2 Delay differential equations

We now briefly recall some basic facts on the theory of DDEs; see Refs. [4,18,30] for further details. Readers may find it useful to look ahead to the concrete example of the PCF laser, system (14) in Section 4. We consider the simplest case, namely an autonomous DDE with a single fixed delay. It has the general form

$$\frac{dx(t)}{dt} = F(x(t), x(t - \tau), \lambda), \quad (1)$$

where $F : \mathbb{R}^n \times \mathbb{R}^n \times \mathbb{R}^p \rightarrow \mathbb{R}^n$ is differentiable and $\tau \in \mathbb{R}^{>0}$ is a fixed delay, while $\lambda \in \mathbb{R}^p$ is a multi-parameter.

We call \mathbb{R}^n the *physical space* of the system. The *phase space* of (1) is the infinite-dimensional space of continuous functions \mathbf{C} defined on the interval $[-\tau, 0]$ with values in \mathbb{R}^n . A *point*, say $q \in \mathbf{C}$, lives in this infinite-dimensional phase space, that is, q is a continuous function

$$q : [-\tau, 0] \rightarrow \mathbb{R}^n. \quad (2)$$

We call $q(0)$ the *headpoint* of q and $q|_{[-\tau, 0)} = \{q(t) \mid t \in [-\tau, 0)\}$ its *history*.

The evolution of a point $q \in \mathbf{C}$ after time $t \geq 0$ is given by the *evolution operator*

$$\Phi^t : \mathbf{C} \rightarrow \mathbf{C}. \quad (3)$$

This is formally given by an abstract differential equation on the infinite-dimensional phase space [5].

A *periodic solution* $\Gamma(t)$ of (1) is a solution which repeats itself after some period $T > 0$, that is $\Gamma(t) = \Gamma(t + T)$ for all t . Each segment $q \in \mathbf{C}$ of Γ , that is $q(\theta) = \Gamma(t + \theta)$ for $\theta \in [-\tau, 0]$, is a *periodic point* of the evolution operator Φ^T , such that $\Phi^T(q) = q$. The periodic orbit Γ traces out a closed curve in projection onto the physical space \mathbb{R}^n ; see already Fig. 2.

For a prescribed section $\Sigma \subset \mathbb{R}^n$ and by denoting \mathbf{C}_Σ as the space of points in \mathbf{C} with headpoints in Σ , then the *Poincaré map* P is defined as

$$P : \mathbf{C}_\Sigma \rightarrow \mathbf{C}_\Sigma, \quad q \mapsto \Phi^{t_q}(q), \quad (4)$$

where $t_q > 0$ is the return time to Σ . After choosing a section Σ (locally) transverse to a periodic orbit Γ , the point $q \in \mathbf{C}_\Sigma$ is a fixed point under P (and a periodic point of (1)).

Near q the map P can be defined as the k th return to Σ for some fixed k , where k counts all intersections of Γ with Σ (of which $k - 1$ are outside a small neighborhood of q). We note that it is generally not possible to define P *globally* as the k th return map to Σ for a fixed k , that is, the flow may fail to be transverse and this changes the number of returns to Σ . (This is in contrast to periodically forced systems, which do have a globally defined Poincaré map in the form of the stroboscopic map of the forcing frequency [3].) Such a tangency can occur at the begin point, an interior point or the end point of the orbit of the flow. We will encounter such tangencies in Section 4.

The stability of Γ is given by its *Floquet multipliers*, which are the solutions of a transcendental eigenvalue problem given by the linearization of (1) around Γ ; see Section 3.1. This linearization is directly connected to the linearization $DP(q)$ of the Poincaré map P at the respective fixed point $q \in \mathbf{C}_\Sigma$: the Floquet multipliers are the eigenvalues of $DP(q)$. We remark that the only exception to this is the so-called ‘trivial’ Floquet multiplier $+1$ of Γ , which is always present and corresponds to the tangent direction to Γ , but does not appear as an eigenvalue of $DP(q)$. It is a crucial property of DDEs that $DP(q)$ is a compact operator, which implies that its spectrum consists of countably many eigenvalues (the Floquet multipliers) with the origin of the complex plane as

their only possible accumulation point; see Refs. [18,30] for more details. In other words, for any fixed $r > 0$ there are only a finite number of Floquet multipliers outside a circle of radius $r > 0$, so that there are always only a finite number of unstable eigendirections (associated with Floquet multipliers outside the unit circle). A periodic orbit is called *hyperbolic* if there are no Floquet multipliers on the unit circle (except for the trivial multiplier). A hyperbolic periodic orbit is either stable if all the Floquet multipliers are inside the unit circle or of *saddle type* with finitely many unstable eigendirections.

If there are other Floquet multipliers (in addition to the trivial multiplier at +1) on the unit circle then the system is undergoing a bifurcation. In this study we will encounter a saddle-node bifurcation of limit cycles which is associated with a real Floquet multiplier crossing the unit circle at +1.

In what follows, we are interested in the one-dimensional *unstable manifold* $W^u(q)$ of a saddle point $q \in \mathbf{C}_\Sigma$ associated with a periodic orbit Γ , with exactly one unstable Floquet multiplier. This is the set of all points $p \in \mathbf{C}_\Sigma$ that can be iterated backwards under P and are such that $P^l(p) \rightarrow q$ as $l \rightarrow -\infty$. The unstable manifold $W^u(q)$ is finite-dimensional and at q it is tangent to the linear eigenspace $E^u(q)$ spanned by the *unstable eigenfunction*. In projection onto the physical space \mathbb{R}^n , the 1D linear eigenspace $E^u(q)$ forms a one-parameter family of directions along (the history of) q ; see already Figs. 1 and 2.

In projection onto the physical space \mathbb{R}^n a 1D unstable manifold $W^u(q)$ forms a complicated object. However, its *trace* $W^u(q) \cap \Sigma$ is a 1D curve that is smooth (except possibly at isolated points due to the projection). It can be interpreted in much the same way as a 1D unstable manifold of a fixed point of a planar map. We remark that as an artifact of the projection, the trace may have self-intersections (reminding one of the fact that $W^u(q)$ lives in an infinite-dimensional phase space).

3 Unstable eigenfunctions and manifold computations

The method presented in Ref. [20] for computing 1D unstable manifolds of saddle periodic orbits in DDEs was developed from that in Ref. [22] for maps. It grows the manifold as a sequence of points $\{p_k\}$, which are all in \mathbf{C}_Σ , where we use linear approximation between neighboring points. The distance between these points is governed by the curvature of the trace of the manifold, which is given by the sequence $\{p_k(0)\}$ of headpoints.

Supposing that the manifold has been computed up to the point p_k , the idea is to find the next point p_{k+1} at a distance Δ_k from the point p_k . This is done

by finding a pre-image \hat{p} of the point p_{k+1} which lies on the computed part of the manifold. By identifying the two points p_l and p_{l+1} between which \hat{p} must lie, \hat{p} is found by bisection. To reduce the number of bisection steps, a small tolerance ε is allowed, meaning that we only require that

$$(1 - \varepsilon)\Delta_k < |P(\hat{p}(0)) - p_k(0)| < (1 + \varepsilon)\Delta_k. \quad (5)$$

The distance Δ_k is adapted during computations according to the curvature of the trace as pre-specified by four accuracy parameters, α_{\min} , α_{\max} , $(\Delta\alpha)_{\min}$ and $(\Delta\alpha)_{\max}$; see Ref. [20] for details. A computation stops after a prescribed arclength of the trace has been reached, or when Δ_k falls below a pre-specified small value, thus detecting convergence to an attracting fixed point.

The starting data needed for a manifold computation is a saddle fixed point $q \in \mathbf{C}_\Sigma$ of the Poincaré map and two points along $W^u(q)$, one on each of the two branches of $W^u(q)$. We work here with the linear approximation to $W^u(q)$ near q and need to find points $q_\delta^\pm \in \mathbf{C}_\Sigma$ at a distance δ from q along the linear unstable eigenspace $E^u(q)$. In particular, this means that $q_\delta^\pm(0) \in \Sigma$. The question is: how can one find q_δ^\pm numerically?

In Ref. [20], we used an iterative power method to find a vector $v \in \mathbf{C}_\Sigma$ approximately spanning $E^u(q)$, normalized so that $|v(t)| = 1$ for all $t \in [-\tau, 0]$. As starting data we used q and $q \pm \delta v$. This works quite well but, in fact, the vector v does not span $E^u(q)$. First of all, the magnitude of the vector spanning $E^u(q)$ varies along Γ , while for our approximation v it is constant; see already Fig. 1. Secondly, $v(0)$ lies in Σ , but in general, $E^u(q)$ has a component pointing out of the section Σ ; see already Fig. 2. We noticed that especially near bifurcations we had difficulties getting the manifold algorithm started. A typical problem is that both $q + \delta v$ and $q - \delta v$ lie on the same side of the stable manifold, so that only one branch of $W^u(q)$ is computed.

The shortcomings of the vector v obtained by the power method motivated the work in this paper. We now explain how a much better starting point for a 1D manifold computation can be found in the form of the first point q_δ^\pm along $E^u(q)$ as defined above. First, we find the respective eigenfunction of the unstable eigenvalue with DDE-BIFTOOL and then use this data to construct q_δ^\pm .

Throughout this paper we use for illustration the DDE describing the PCF laser introduced in Section 4, where we consider the fixed section

$$\Sigma \equiv \{ (E, N) \mid E_x = 0 \}. \quad (6)$$

3.1 Approximating the unstable eigendirection

In order to compute the unstable eigenfunction of the Poincaré operator $DP(q)$ corresponding to a periodic solution Γ we consider the linearization of (1) around Γ , given by

$$\frac{dy(t)}{dt} = A(t)y(t) + B(t)y(t - \tau) \quad (7)$$

where we have omitted the dependency on λ (which is considered to be fixed in this section). The periodic coefficients A , B are defined as (writing $F \equiv F(x_1, x_2, \lambda)$)

$$A(t) = \frac{\partial F}{\partial x_1}|_{(\Gamma(t), \Gamma(t-\tau), \lambda)} \quad \text{and} \quad B(t) = \frac{\partial F}{\partial x_2}|_{(\Gamma(t), \Gamma(t-\tau), \lambda)}. \quad (8)$$

The evolution operator of the linearized equations (7) is given by

$$D\Phi^t : \mathbf{C} \rightarrow \mathbf{C}. \quad (9)$$

The eigenvalues of $D\Phi^T$, where T is the period of Γ , are the Floquet multipliers μ of the periodic solution. The operator $D\Phi^T$ has only a point spectrum (except possibly for the eigenvalue zero). Hence, for each $\mu \neq 0$ there exists a corresponding eigenfunction segment $q_\mu \in \mathbf{C}$, such that,

$$D\Phi^T q_\mu = \mu q_\mu. \quad (10)$$

Moreover, it follows that q_μ is an eigenfunction segment of a trajectory y_μ which repeats itself after time T scaled by the factor μ ,

$$y_\mu(t + T) = \mu y_\mu(t) \quad \text{for all } t. \quad (11)$$

DDE-BIFTOOL is a Matlab package of routines for the bifurcation analysis of DDEs; see Ref. [8] for details. Within DDE-BIFTOOL, we approximate the flow (7) and correspondingly the operator $D\Phi^T$ by using collocation equations. (Except for the time dependency in (7), this scheme is completely equivalent to the collocation equations used for obtaining the periodic solution Γ itself.)

The periodic solution Γ is approximated by a piecewise polynomial solution on $[0, T]$ represented on the time-scaled mesh $\{t_0 = 0 < t_1 < \dots < t_L = 1\}$ as a polynomial p_i of degree d on each sub-interval $[t_i, t_{i+1}]$, $i = 0, \dots, L - 1$.

It is continuously linked at the sub-interval boundaries, $p_i(t_{i+1}) = p_{i+1}(t_{i+1})$. Note that this representation is uniquely determined by its values $x_{i+\frac{j}{d}}$ at $t_{i+\frac{j}{d}}$, $i = 0, \dots, L-1$, $j = 0, \dots, d-1$, so that p_i is the Lagrange interpolating polynomial through $x_{i+\frac{j}{d}}$, $j = 0, \dots, d$.

To construct a corresponding approximation q_i for $y_\mu(t)$, we impose d collocation equations within each sub-interval, namely

$$\dot{q}_i(c_{i,j}) = \begin{cases} \mathbb{T}f(q_i(c_{i,j}), q_i(c_{i,j} - \tau/\mathbb{T} + 1), \lambda) & \text{when } c_{i,j} < \tau/\mathbb{T} \\ \mathbb{T}f(q_i(c_{i,j}), q_i(c_{i,j} - \tau/\mathbb{T}), \lambda) & \text{when } c_{i,j} \geq \tau/\mathbb{T} \end{cases} \quad (12)$$

where we introduced $c_{i,j} = t_i + c_j(t_{i+1} - t_i)$ for notational convenience, and $c_j \in [0, 1]$ are the collocation constants; see Ref. [7] for more details. These equations can be used to obtain a discrete mapping (a matrix M) of the approximation on the function segment $[-\tau/\mathbb{T}, 0]$ to the approximation on the function segment $[1 - \tau/\mathbb{T}, 1]$ (notice the scaling of time), where we use a periodic extension of the mesh, $t_{-i} = t_{L-i} - 1$. The eigenvalues of this matrix M can then be computed and they approximate the Floquet multipliers. The convergence of the multiplier approximations was investigated in Ref. [24]. Likewise, the eigenvectors of M are discrete approximations of the eigenfunction segments q_μ on $[-\tau, 0]$. Once an approximation is known on $[-\tau/\mathbb{T}, 0]$, these eigenfunction segments are expanded using the collocation equations (12), which can be solved on $[0, 1]$. In this way, we obtain an approximation of y_μ on $[-\mathbb{T}, 0]$. Note that this eigenfunction approximation is not periodic on $[-\mathbb{T}, 0]$, a fact that we will revisit in Section 3.2.

Since the collocation mesh used in (7) for obtaining the approximate eigendirections is exactly the same as the one used for obtaining Γ , approximations of Γ at the mesh points used in the discretization of (7) are readily available. We remark that refining the mesh for computing the eigendirection compared to the mesh for obtaining Γ does not appear to be sensible, because the overall accuracy is limited in any case by the accuracy of the approximation obtained for Γ .

The above scheme is now implemented as part of DDE-BIFTOOL. For a given Floquet multiplier μ the user has access to the eigentrajectory y_μ over the period interval $[-\mathbb{T}, 0]$ of Γ . This is useful in several situations, for example, when switching between branches of periodic orbits at bifurcation points and indeed to generate starting data for 1D unstable manifold computations.

3.2 Constructing q_δ^\pm

The first step is to obtain DDE-BIFTOOL data for Γ such that it is given as a function over the period interval $[-T, 0]$ so that the head point $\Gamma(0)$ lies in the section Σ . This is easily achievable by giving DDE-BIFTOOL the extra condition that the headpoint must lie in Σ when computing and correcting the orbit. Γ and y_μ represented in this way constitute the ‘raw data’ we need.

Figure 1 shows a saddle periodic orbit Γ of the PCF laser with one unstable Floquet multiplier μ , together with the associated unstable eigenfunction $E^u(\Gamma)$ given by $(\Gamma + \delta y_\mu)(t)$ for any $\delta \in \mathbb{R}$. (In the figure we used the value of $\delta = 3.0$, so that ‘one side’ of $E^u(\Gamma)$ is shown, and plot the three components E_x , E_y and N separately.) The length of the vector $(\Gamma + \delta y_\mu)(0)$ at $\Gamma(0)$ is approximately $\mu = 3.14897$ times that of $(\Gamma + \delta y_\mu)(-T)$ at $\Gamma(-T)$, illustrating that the Floquet multiplier μ measures the linear expansion over one period T . Notice that $\Gamma_{E_x}(0) = 0$, which means that Γ indeed lies in the section Σ defined by (6).

Figures 2 (a) and (b) show the same data as Fig. 1, but now plotted in projection onto (E, N) -space and the E -plane, respectively. Similarly, Fig. 2 (c) and (d) shows the respective data for $\delta = -3.0$, that is, the ‘other side’ of $E^u(\Gamma)$. Also plotted in bold are the points q_δ^+ and q_δ^- that we are seeking, whose headpoints lie in Σ . It is immediately apparent from this figure, that

$$q_\delta^\pm \neq q \pm \delta q_\mu \quad (13)$$

where q is the fixed point associated with Γ and q_μ the respective eigenfunction, both over the interval $[-\tau, 0]$.

The desired points q_δ^+ and q_δ^- can be extracted from the raw data as follows. In the first case, sketched in Fig. 2 (a) and (b), the vector $y_\mu(0)$ points in the same direction as the flow. This means that the point $(\Gamma + \delta y_\mu)(0)$ lies past the section Σ . In this situation, the desired point q_δ^+ can be found by moving backwards (by decreasing t) along the data $\Gamma + \delta y_\mu$ and find by interpolation the (first) intersection point of this data with Σ . This point is by definition $q_\delta^+(0)$ and the data segment of length τ before this point is q_δ^+ .

The second case is shown in Figs. 2 (c) and (d). Here $(\Gamma + \delta y_\mu)(0)$ points in the opposite direction to the flow, so that $(\Gamma + \delta y_\mu)(0)$ lies before the section Σ . In this situation, the desired point q_δ^+ must be found by moving forward, that is, by increasing t . The problem is that $\Gamma + \delta y_\mu$ is only known in the time interval $[-T, 0]$. To obtain data for $t > 0$ we extend the data for Γ simply by periodicity. However, the data for y_μ is not periodic, owing to the expansion given by the Floquet multiplier μ . Nevertheless, we can extend the data for y_μ by periodicity if we multiply by μ at the same time, hence, using the scaling

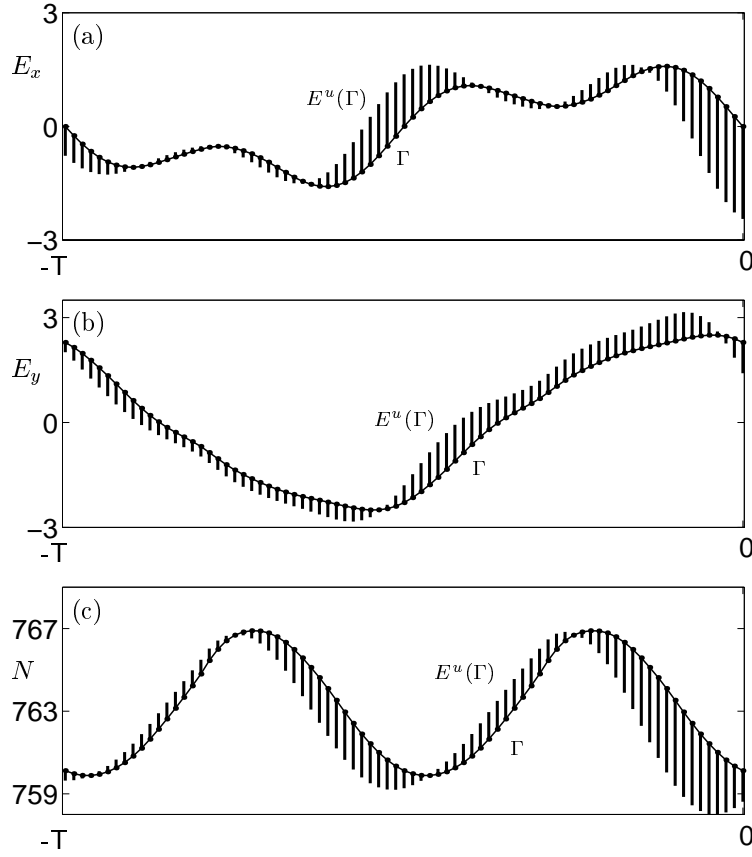


Fig. 1. Time traces over one period T of the components E_x (a), E_y (b) and N (c) of the saddle periodic orbit Γ together with $\Gamma + \delta y_\mu$ for $\delta = 3.0$, illustrating one branch of the unstable linear eigenspace $E^u(\Gamma)$.

(11). Once the data has been extended in this way, we move forward in the data, find the intersection point $q_\delta^+(0)$ with Σ by interpolation and obtain q_δ^+ as the data segment of length τ before this point.

This procedure is now fully implemented in Matlab, so that it is integrated with the DDE-BIFTOOL routines. As output we write out both q and q_δ^\pm for the δ that was specified by the user. This output forms the starting data as needed by the 1D manifold algorithm introduced in Ref. [20].

The fact that the vector $q_\mu(0)$ generically points out of the section Σ has the consequence that the intersection of the linear space $E^u(\Gamma)$ with the plane Σ is not a straight line. The two branches of this intersection curve are given by the parametrized families $\{q_\delta^\pm(0) \mid \delta \in \mathbb{R}\}$, which is shown in Fig. 3. Also shown is part of the global 1D unstable manifold W^u computed using our algorithm with an initial perturbation of $\delta = 0.001$. It is clear that $E^u(\Gamma) \cap \Sigma$ is indeed not a straight line, but a curve that is tangent to W^u at q . (Note that at q , $E^u(q)$ is tangent to $W^u(q)$ not only at $q(0)$ but also along the entire history of q .) Notice that for large values of δ , the linear space $E^u(\Gamma)$ is in

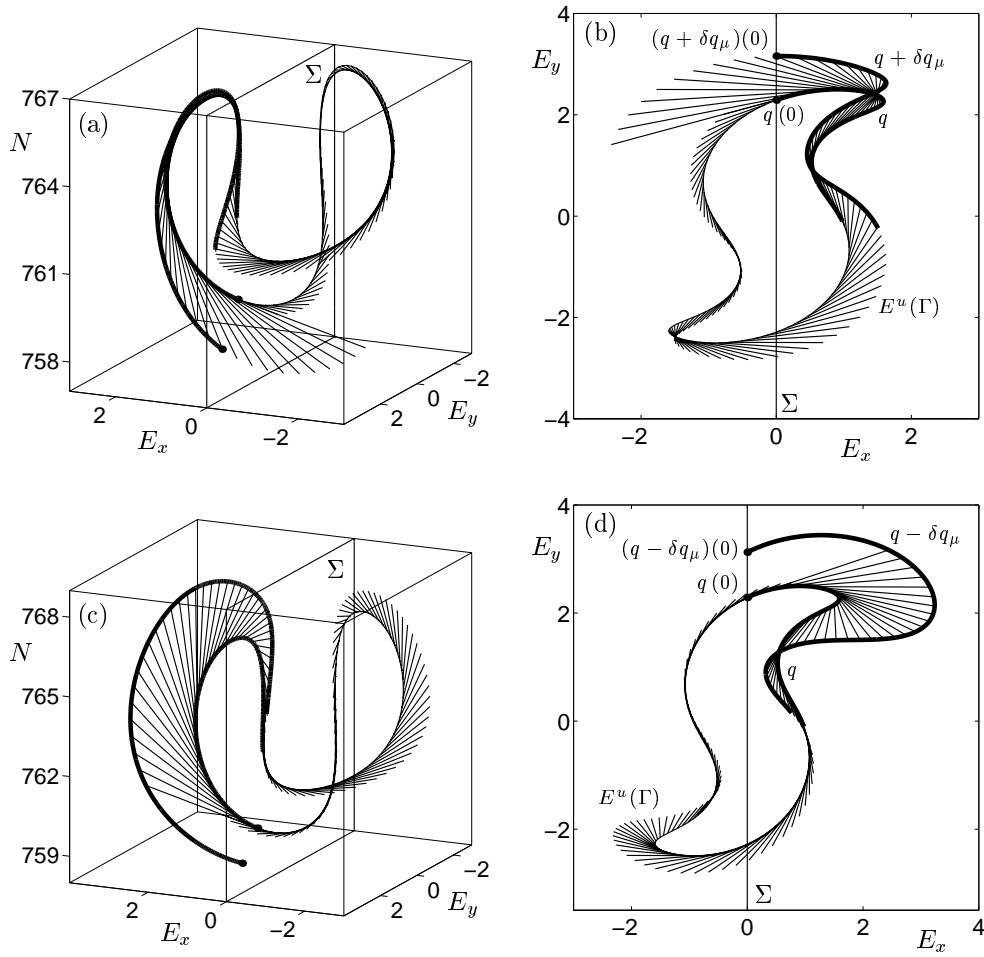


Fig. 2. The saddle periodic orbit Γ from Fig. 1 together with $\Gamma + \delta y_\mu$, for $\delta = 3.0$ in panels (a) and (b), and for $-\delta = 3.0$ in panels (c) and (d), shown in projection onto (E, N) -space and E -space, respectively. Also shown are the points q_δ^\pm for $\delta = 3.0$.

very bad approximation to the 1D unstable manifold W^u ; see Fig. 3 (b). It is therefore very important to choose δ small enough when starting a manifold computation. In Figs. 1 and 2 we chose $\delta = 3$ purely for illustrative purposes. Figure 3 (b) shows that an initial distance of $\delta = 3$ along $E^u(\Gamma)$ would give very bad starting data for computing the manifold $W^u(\Gamma)$.

4 Example: PCF laser

For illustration we consider the technologically relevant example of a DDE describing a PCF laser [11,19]. This system can be modelled by the following delay differential equations

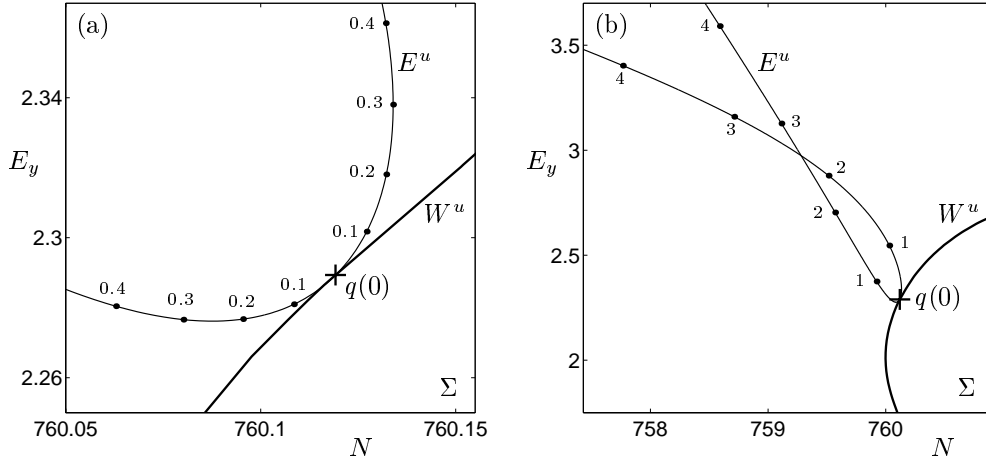


Fig. 3. Unstable linear eigenspace $E^u(q)$ as parametrized by $\{q_\delta^\pm(0) \mid \delta \in \mathbb{R}\}$, together with the unstable manifold $W^u(q)$ as computed with our algorithm (for an initial distance of $\delta = 0.001$); individual dots are for the stated values of δ .

$$\begin{aligned} \frac{dE}{dt} &= \frac{1}{2} \left[-i\alpha G_N(N(t) - N_{\text{sol}}) + \left(G(t) - \frac{1}{\tau_p} \right) \right] E(t) + \kappa E^*(t - \tau) \quad (14) \\ \frac{dN}{dt} &= \frac{I}{q} - \frac{N(t)}{\tau_e} - G(t) |E(t)|^2 \end{aligned}$$

describing the evolution of the complex electric field $E(t) = E_x(t) + iE_y(t)$ and the population inversion $N(t)$. Nonlinear gain is included in the term $G(t) = G_N(N(t) - N_0)(1 - \epsilon P(t))$ where $\epsilon = 3.57 \times 10^{-8}$ is the nonlinear gain coefficient and $P(t) = |E(t)|^2$ is the intensity. All other parameters were set to realistic values corresponding to a Ga-Al-As semiconductor laser and are given in Refs. [13–16, 19, 20]. The phase-conjugate feedback term involves the feedback rate κ and the external cavity round-trip time τ , which we fix at the realistic value of $\tau = 2/3$ ns, corresponding to an external cavity length $L_{\text{ext}} \approx 10$ cm. We consider changes in the dynamics of the PCF laser as the dimensionless parameter $\kappa\tau$ is varied. Finally, we note that (14) has \mathbb{Z}_2 -symmetry given by the transformation $(E, N) \rightarrow (-E, N)$. Consequently, every invariant set is either symmetric or has a symmetric counterpart under this symmetry.

4.1 General dynamics of the PCF laser

In Ref. [19], it was shown that the general picture of the dynamics of the PCF laser is that of stable periodic operation interspersed with ‘bubbles’ of more complicated, for the most part chaotic dynamics. One refers to these stable periodic orbits as external cavity modes (ECMs) of the PCF laser [13]. The bubbles of chaotic dynamics are the result of competition between ECMs.

The transitions between ECMs and the regions of chaos have been shown to be very sudden. One such transition was studied in Ref. [15] where the transition at the start of the second bubble of chaos, from a locked periodic solution to a chaotic solution, was shown to be due to the break-up of a torus culminating in a crisis bifurcation. This study employed manifold computations to identify the shape of the underlying torus as one passed through the region of locking before the crisis bifurcation and the ensuing chaotic dynamics.

The bifurcation diagram in Fig. 4 (a) shows the first bubble of chaos in the PCF laser. It was obtained by simulation, where we plot, after transients have died down, the normalized inversion N whenever the power $I(t) = |E(t)|^2$ crosses its average value; compare Refs. [15,19]. Figure 4 (a) reveals a steady state locked solution for $\kappa\tau < 0.75$. Physically this corresponds to a frequency match between the solitary laser and the phase-conjugating mirror; see Refs. [13,14,16] for detailed studies of this locked solution. A periodic solution then appears which is seen to undergo a period-doubling route to the first bubble of chaos. One then observes a sudden transition to the first ECM solution at $\kappa\tau \approx 1.86$.

An enlargement of the bifurcation diagram near this transition is shown in Fig. 4 (b). Note that there is no hysteresis in this sudden transition, so that when decreasing $\kappa\tau$ one sees a sudden transition from periodic output to chaos. Figure 4 (b) reveals that the curve of stable periodic solutions has a quadratic tangency with the chaotic region, which is typical for a saddle-node bifurcation of periodic orbits. This phenomenon was already found in Ref. [19] at the end of the second bubble of chaos, where it was identified as an intermittent transition (or a saddle-node bifurcation of periodic orbits that takes place *on* a chaotic attractor). The saddle-node bifurcation itself was found in Ref. [13] by a continuation study of the periodic solutions of the PCF laser.

4.2 Intermittent transition to chaos

In this paper we use manifold computations to show that the sudden transition to periodic operation at the end of the first bubble of chaos is indeed due to an intermittent transition. Specifically, we compute the unstable manifold associated with the saddle periodic solution born in the saddle-node bifurcation of periodic orbits. Due to the closeness of the bifurcation one needs good starting data, and this is where we failed in earlier attempts with the iterative power method. However, the method presented in Section 3 does indeed allow to compute these manifolds.

Figure 5 shows the trace in the section Σ defined by $E_x = 0$ of the unstable manifold $W^u(q)$ of the saddle fixed point q for four values of $\kappa\tau$ as one

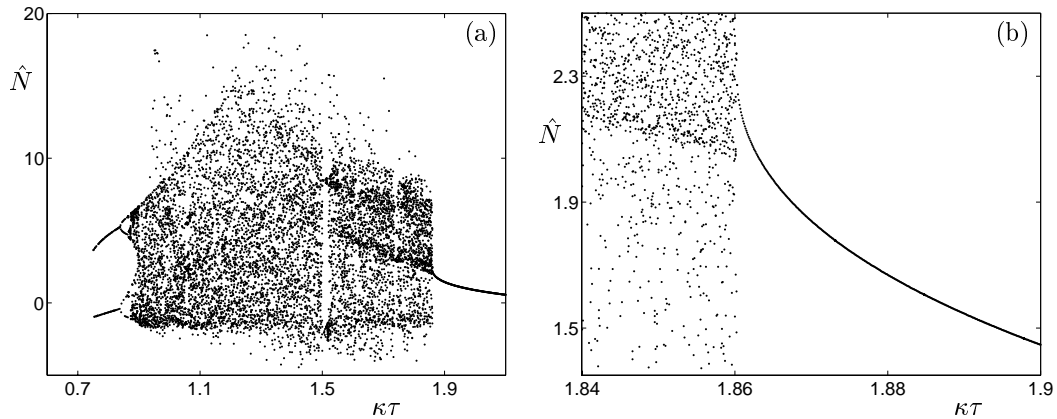


Fig. 4. Bifurcation diagrams of the PCF laser obtained by simulation.

moves away from the saddle-node bifurcation at $\kappa\tau \approx 1.86027$. The horizontal cross (+) indicates the point $q(0)$, while the intersection of the bifurcating stable periodic solution with Σ is marked by a diagonal cross (\times). In each computation, an initial step q_δ^\pm for $\delta = 0.001$ along $E^u(q)$ was used. Other accuracy parameters, detailed in Ref. [20], were set to $\alpha_{\min} = 0.2$, $\alpha_{\max} = 0.3$, $(\Delta\alpha)_{\min} = 5.0 \times 10^{-4}$, $(\Delta\alpha)_{\max} = 5.0 \times 10^{-3}$, $\Delta_{\min} = 5.0 \times 10^{-2}$ and $\varepsilon = 0.2$.

In each panel of Fig. 5, a short branch of the unstable manifold converges to the stable periodic solution (\times). The other branch, on the other hand, is very long and makes very large excursions, where it follows the previous chaotic attractor. To illustrate this, we show the intersection of this chaotic attractor with Σ as a cloud of grey dots. (Note that for the used values of $\kappa\tau$ past the bifurcation at $\kappa\tau \approx 1.86027$ the chaotic attractor does not exist any longer; it is plotted strictly for illustration and is the same in all panels of Fig. 5.) Figure 5 (a) shows the unstable manifold for $\kappa\tau \approx 1.86036$, closest to the saddle-node bifurcation. Here we see that the short branch converges quickly to the stable periodic solution while the long branch follows the old chaotic attractor. As one moves away from the transition, the short branch grows in length but always converges to the stable periodic solution, as is expected near a saddle-node bifurcation. The long branch does not change so much, and principally follows the old chaotic attractor; see Figs. 5 (b), (c) and (d). This shows that we are indeed dealing with an intermittent transition: as one moves towards the bifurcation point, the saddle periodic orbit and the stable periodic orbit get closer together; at the transition the periodic orbits disappear and the long branch of the unstable manifold forms the chaotic attractor.

The reader will notice a ‘gap’ in the upper right of the unstable manifold shown in Figs. 5 (a), (b) and (c). This gap shortens as $\kappa\tau$ is increased and finally closes in Fig. 5 (d). As was described in Ref. [20], it is due to the orbit of the flow becoming tangent to the section Σ . If this tangency occurs at an interior point of the flow, our algorithm changes the number of returns

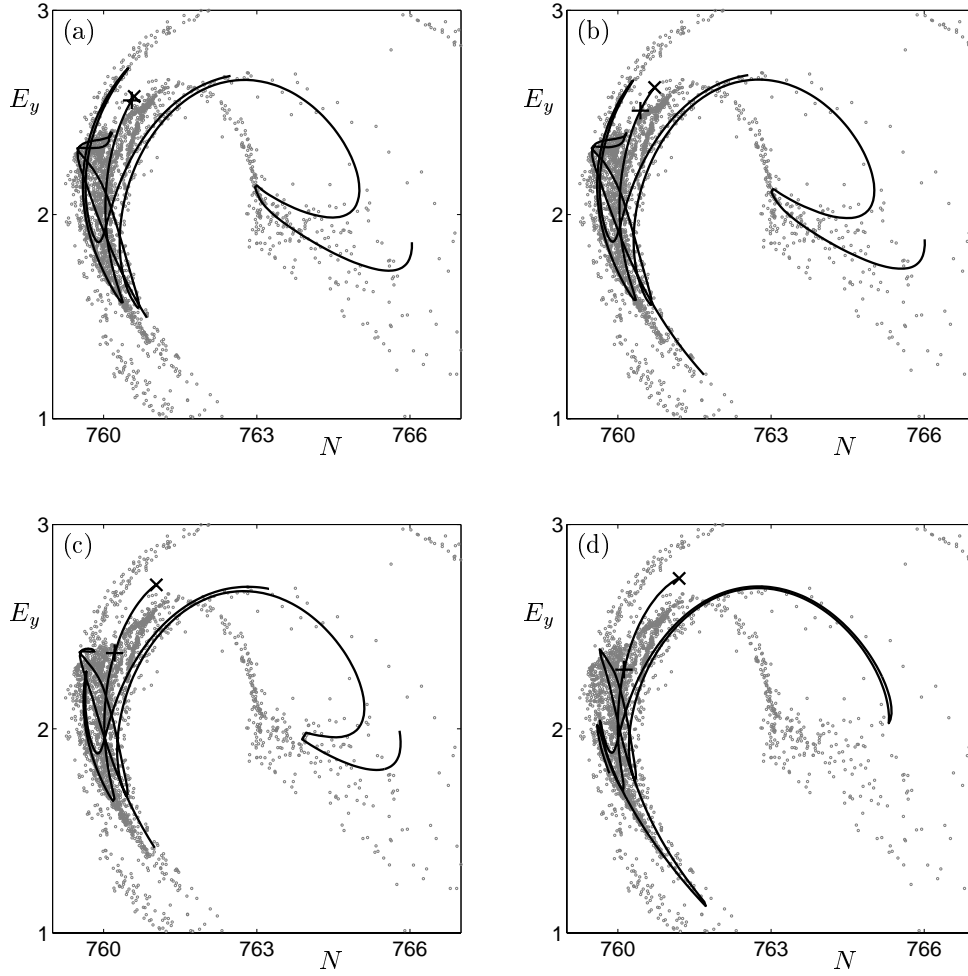


Fig. 5. Both branches of the 1D unstable manifold of the saddle point (+), the short branch converges to the attractor (\times), and the chaotic attractor (grey) that exists before the crisis. From (a) to (d) $\kappa\tau$ takes the values 1.86036, 1.86238, 1.87774 and 1.89159.

of the Poincaré map to Σ and the computation continues. The tangencies are detected by monitoring the integration time used in computing previous points on the manifold. If the tangency occurs at the end point of the orbit of the flow an integration time constraint causes the manifold computation to stop. The gaps in the manifolds of Figs. 5 (a), (b) and (c) are due to a tangency at an end point. However, by applying a large enough time constraint, the algorithm continues to search for new images in Σ of the previously computed part of the manifold and resumes computing the manifold. If this is the case, constraint (5) is ignored, resulting in a gap in the manifold. It is important to check the orbit in phase-space to ensure that the correct branch is being continued and that there has not been a jump to a different branch. The fact that the discontinuous branches match up in panel (d) is conclusive evidence that this approach worked for the present example. In the computations of Figs. 5 an error bound of 20 % was used on subsequent integration times.

5 Conclusions

We used the continuation package DDE-BIFTOOL to compute unstable eigenfunctions of saddle periodic orbits. From these eigenfunctions we then constructed the starting data for 1D unstable manifold computations. We believe this to be the first time that unstable eigenfunctions have been accurately computed and used in DDEs. Our method of generating starting data can be used conjunction with any algorithm for computing unstable manifolds in DDEs, for example, fundamental domain iteration [20,27].

The improved starting data allows one to perform manifold computations in situations where the iterative power method we used previously in Refs. [15,20] ran into difficulty. As an example, we investigated a sudden transition to chaos in a semiconductor laser subject to phase-conjugate feedback and were able to show that this transition was due to a saddle-node bifurcation of limit cycles taking place on the chaotic attractor, known as an intermittent transition.

We expect the study of global dynamics and bifurcations in DDEs arising in applications to be a topic of much interest in the coming years. The algorithm for computing unstable manifolds with starting data obtained from DDE-BIFTOOL as explained here will be a valuable tool. In the near future, we plan to fully integrate the manifold computations with DDE-BIFTOOL into a single software package.

The approach taken here to generate starting data can be generalized to the case of more unstable eigenfunctions. The next challenging step is to generalize the algorithm in Ref. [23] to compute 2D unstable manifolds of equilibria and saddle periodic orbits in DDEs.

Acknowledgments

The work of KG was funded in part by the University of Bristol; he is now a Fellow of the Fund for Scientific Research, Flanders (Belgium). BK was supported by an EPSRC Advanced Research Fellowship.

References

- [1] G. P. Agrawal and G. R. Gray. Effect of phase-conjugate feedback on the noise characteristics of semiconductor lasers. *Phys. Rev. A*, 46:5890–5898, 1992.
- [2] C. T. H. Baker, G. A. Bocharov, and F. A. Rihan. A report on the use of delay differential equations in numerical modelling in the biosciences. Technical Report 343, Department of Mathematics, University of Manchester, July 1999.

- [3] H. W. Broer and B. Krauskopf. Chaos in periodically driven systems. In [21], pp. 31–53.
- [4] O. Diekmann, S. A. Van Gils, S. M. Verduyn Lunel, and H. O. Walther. *Delay Equations: Functional-, Complex-, and Nonlinear Analysis*, volume 110. Springer-Verlag, 1995.
- [5] K. J. Engel and R. Nagel. *One-parameter semigroups for linear evolution equations*, volume 194 of *Graduate texts in mathematics*. Springer-Verlag, New York, 2000.
- [6] K. Engelborghs, V. Lemaire, J. Bélair, and D. Roose. Numerical bifurcation analysis of delay differential equations arising from physiological modeling. *J. Math. Biol.*, 42:361–385, 2001.
- [7] K. Engelborghs, T. Luzyanina, K. in’t Hout, and D. Roose. Collocation methods for the computation of periodic solutions of delay differential equations. *SIAM J. Sci. Comput.*, 22:1593–1609, 2000.
- [8] K. Engelborghs, T. Luzyanina, and G. Samaey. DDE-BIFTOOL v2.00: a Matlab package for bifurcation analysis of delay differential equations. Technical Report TW-330, Department of Computer Science, K. U. Leuven, Belgium, 2000. <http://www.cs.kuleuven.ac.be/~koen/delay/ddebiftool.shtml>.
- [9] I. R. Epstein and J. A. Pojman. *An Introduction to Non-linear Chemical Oscillations*. Oxford University Press, New York, 1998.
- [10] G. R. Gray, D. H. DeTienne, and G. P. Agrawal. Mode locking in semiconductor lasers by phase-conjugate optical feedback. *Opt. Lett.*, 20:1295–1297, 1995.
- [11] G. R. Gray, D. Huang, and G. P. Agrawal. Chaotic dynamics of semiconductor lasers with phase-conjugate feedback. *Phys. Rev. A*, 49:2096–2105, 1994.
- [12] C. Grebogi, E. Ott, F. Romeiras, and J. A. Yorke. Critical exponents for crisis-induced intermittency. *Phys. Rev. A*, 36:5365–5380, 1987.
- [13] K. Green and B. Krauskopf. Bifurcation analysis of frequency locking in a semiconductor laser with phase-conjugate feedback. *Int. J. Bif. Chaos*, to appear.
- [14] K. Green and B. Krauskopf. Global bifurcations and bistability at the locking boundaries of a semiconductor laser with phase-conjugate feedback. *Phys. Rev. E*, 66(016220), 2002.
- [15] K. Green, B. Krauskopf, and K. Engelborghs. Bistability and torus break-up in a semiconductor laser with phase-conjugate feedback. *Phys. D*, 173:114–129, 2002.
- [16] K. Green, B. Krauskopf, and G. Samaey. A two-parameter study of the locking region of a semiconductor laser subject to phase-conjugate feedback. *SIAM J. Applied Dynamical Systems*, in press

- [17] B. Haegeman, K. Engelborghs, D. Roose, D. Pieroux, and T. Erneux. Stability and rupture of bifurcation bridges in semiconductor lasers subject to optical feedback. *Phys. Rev. E*, 66(046216), 2002.
- [18] J. K. Hale and S. M. Verduyn Lunel. *Introduction to Functional Differential Equations*. Springer-Verlag, 1993.
- [19] B. Krauskopf, G. R. Gray, and D. Lenstra. Semiconductor laser with phase-conjugate feedback: Dynamics and bifurcations. *Phys. Rev. E*, 58:7190–7196, 1998.
- [20] B. Krauskopf and K. Green. Computing unstable manifolds of periodic orbits in delay differential equations. *J. Comput. Phys.*, 186:230–249, 2003.
- [21] B. Krauskopf and D. Lenstra, editors. *Fundamental Issues of Nonlinear Laser Dynamics*, volume 548. AIP Conf. Proc., 2000.
- [22] B. Krauskopf and H. M. Osinga. Growing 1D and quasi 2D unstable manifolds of maps. *J. Comp. Phys.*, 146:404–419, 1998.
- [23] B. Krauskopf and H. M. Osinga. Globalizing two-dimensional unstable manifolds of maps. *Int. J. Bif. Chaos*, 8:483–503, 1998.
- [24] T. Luzyanina and K. Engelborghs. Computing Floquet multipliers for functional differential equations. *Int. J. Bif. Chaos*, to appear.
- [25] P. Manneville and Y. Pomeau. Different ways to turbulence in dissipative dynamical systems. *Phys. D*, 1(2):219–226, 1980.
- [26] J. D. Murray. *Mathematical Biology*, volume 19. Springer-Verlag, Berlin, 1980.
- [27] T. S. Parker and L. O. Chua. *Practical Numerical Algorithms for Chaotic Systems*. Springer-Verlag, New York/Berlin, 1991.
- [28] M. Sciamanna, T. Erneux, F. Rogister, O. Deparis, P. Megret, and M. Blondel. Bifurcation bridges between external-cavity modes lead to polarization self-modulation in vertical-cavity surface-emitting lasers. *Phys. Rev. A*, 65(041801(R)), 2002.
- [29] G. H. M. Van Tartwijk and G. P. Agrawal. Laser instabilities: a modern perspective. *Prog. Quantum Electron.*, 22:43–122, 1998.
- [30] S. M. Verduyn Lunel and B. Krauskopf. The mathematics of delay equations with an application to the Lang-Kobayashi equations. In [21], pp. 66–86.